Preclinical Evaluation of ^{225}Ac-Labeled Single Domain Antibody for the Treatment of HER2^{pos} Cancer

Magdalena Rodak[1,†], Yana Dekempeneer[2,†], Maria Wojewódzka[1], Vicky Caveliers[2,3], Peter Covens[2], Brian W. Miller[4], Matthijs B. Sevenois[2], Frank Bruchertseifer[5], Alfred Morgenstern[5], Tony Lahoutte[2,3], Matthias D'Huyvetter[2,*], Marek Pruszyński[1,6,*]

[1] Institute of Nuclear Chemistry and Technology, Warsaw, Poland

[2] Department of Medical Imaging, In Vivo Cellular and Molecular Imaging Laboratory, Vrije Universiteit Brussel, Brussels, Belgium

[3] Nuclear Medicine Department, UZ Brussel, Brussels, Belgium

[4] Department of Medical Imaging, University of Arizona, Tucson, Arizona, USA

[5] European Commission, Joint Research Centre (JRC), Karlsruhe, Germany

[6] NOMATEN Centre of Excellence, National Centre for Nuclear Research, Otwock, Poland

[†] Authors contributed equally

* Authors share senior authorship

Running title: Targeted Alpha Therapy of HER2-positive cancer.

Corresponding authors: Marek Pruszyński, Dorodna 16, 03-195 Warsaw, Phone: +48-22-504-1085, E-mail: m.pruszynski@ichtj.waw.pl, ORCID: 0000-0001-8835-2462; Matthias D'Huyvetter, Laarbeeklaan 103, B-1090 Brussels, Phone: +32-2-477-49-91, E-mail: matthias.dhuyvetter@vub.be

Conflict of interest disclosures: Y. Dekempeneer and M. D'Huyvetter are employees and T. Lahoutte is consultant of Precirix NV and hold ownership interest (including patents) in sdAb radiotherapeutics. T. Lahoutte is member of the scientific advisory board of Ion Beam Applications (IBA) and member of the strategic committee of the Institute of RadioElements (IRE). No additional potential conflict of interest relevant to this article was reported.

Downloaded from http://aacrjournals.org/mct/article-pdf/doi/10.1158/1535-7163.MCT-21-1021/3208456/mct-21-1021.pdf by Instytut Marii Sklodowskiej-Curie Oddzial w. Gliwicach user on 10 October 2022

Abstract

Human epidermal growth factor receptor type 2 (HER2) is overexpressed in various cancers; thus, HER2-targeting single-domain antibodies (sdAbs) could offer a useful platform for radioimmunotherapy. In this study, we optimized the labeling of an anti-HER2-sdAb with the α-particle-emitter ^{225}Ac through a DOTA-derivative. The formed radioconjugate was tested for binding affinity, specificity and internalization properties, whereas cytotoxicity was evaluated by clonogenic and DNA double-strand-breaks assays. Biodistribution studies were performed in mice bearing subcutaneous HER2^{pos} tumors to estimate absorbed doses delivered to organs and tissues. Therapeutic efficacy and potential toxicity were assessed in HER2^{pos} intraperitoneal ovarian cancer model and in healthy C57Bl/6 mice.

[^{225}Ac]Ac-DOTA-2Rs15d exhibited specific cell uptake and cell-killing capacity in HER2^{pos} cells (EC_{50} = 3.9±1.1 kBq/mL). Uptake in HER2^{pos} lesions peaked at 3 h (9.64±1.69% IA/g), with very low accumulation in other organs (< 1% IA/g) except for kidneys (11.69±1.10% IA/g). α-camera imaging presented homogeneous uptake of radioactivity in tumors, although heterogeneous in kidneys, with a higher signal density in cortex versus medulla. In mice with HER2^{pos} disseminated tumors, repeated administration of [^{225}Ac]Ac-DOTA-2Rs15d significantly prolonged survival (143 days) compared to control groups (56 days and 61 days) and to the group treated with HER2-targeting mAb trastuzumab (100 days). Histopathological evaluation revealed signs of kidney toxicity after repeated administration of [^{225}Ac]Ac-DOTA-2Rs15d.

[^{225}Ac]Ac-DOTA-2Rs15d efficiently targeted HER2^{pos} cells and was effective in treatment of intraperitoneal disseminated tumors, both alone and as an add-on combination with trastuzumab, albeit with substantial signs of inflammation in kidneys. This study warrants further development of [^{225}Ac]Ac-DOTA-2Rs15d.

Downloaded from http://aacrjournals.org/mct/article-pdf/doi/10.1158/1535-7163.MCT-21-1021/3208456/mct-21-1021.pdf by Instytut Marii Sklodowskiej-Curie Oddzial w. Gliwicach user on 10 October 2022

Introduction

Targeted Alpha Therapy (TAT) exploits a combination of an α-particle emitting radionuclide and a targeting moiety, that allows specific delivery of cytotoxic radiation to cancerous cells. Due to their limited path length, α-particles are of particular interest for the treatment of residual and metastatic diseases. Several relevant radionuclides for TAT are currently under (pre-)clinical evaluation (1,2). ^{225}Ac ($t_{1/2}$ = 9.9 days) is an interesting radionuclide due to the emission of four α-particles in its decay chain with a total deposited α-energy of 27.6 MeV. Several clinical trials have shown high potential of ^{225}Ac-based TAT to treat advanced cancers (3,4). It has recently been demonstrated that TAT with [^{225}Ac]Ac-PSMA-617 could overcome emerging radio-resistance to β^--particle radiation. Moreover, the shorter range of α-particles in tissue impacts hematologic toxicity in treated patients with diffuse red marrow infiltration as these particles cause less toxicity compared to β^--emitting radionuclides such as ^{90}Y and ^{177}Lu, which release cytotoxic particles with significant longer path lengths (5,6).

Several ^{225}Ac-labeled monoclonal antibodies (mAbs) are being investigated in Phase I/II clinical trials to treat hematological cancers (7,8). However, the success of mAb-based TAT in epithelial solid tumors is limited due to toxicities in well-perfused organs. High binding affinity and specificity, fast clearance from blood and the ability to homogeneously distribute in target tissues make small-sized single-domain antibodies (sdAbs) promising targeting molecules for TAT (9–12). Previously, a HER2-targeting sdAb was successfully radiolabeled with therapeutic radioisotopes such as ^{225}Ac, ^{211}At, and ^{177}Lu (10,11,13). [^{225}Ac]Ac-DOTA-2Rs15d was found to be effective in inhibiting the HER2^{pos} cells proliferation in a dose-dependent manner and *in vivo* accumulated in a HER2^{pos} tumor in a specific way (10), with uptake values comparable to what has been measured for its ^{177}Lu-labeled counterpart (13). However, in contrast to the ^{177}Lu-labeled variant, elevated liver uptake was observed, likely due to ^{225}Ac non-specifically bound to the sdAb, which might have resulted in an *in vivo* dissociation and accumulation in liver, as noticed earlier (10). In addition, it was shown to be effective in mice bearing intracranial HER2^{pos} tumor xenografts (14). In this study, the same sdAb was radiolabeled with ^{225}Ac using optimized reaction conditions, and fully

Downloaded from http://aacrjournals.org/mct/article-pdf/doi/10.1158/1535-7163.MCT-21-1021/3208456/mct-21-1021.pdf by Instytut Marii Sklodowskiej-Curie Oddzial w. Gliwicach user on 10 October 2022

characterized *in vitro*, after which its therapeutic efficacy was assessed in mice with intraperitoneal HER2^{pos} tumor xenografts.

Materials and Methods

Preparation of [^{225}Ac]Ac-DOTA-sdAbs

All reagents were at least analytical grade and purchased from Sigma Aldrich (St. Louis, MO), unless stated otherwise. ^{225}Ac was obtained from ^{229}Th source by radiochemical separation (15). The HER2-targeting sdAb 2Rs15d (PDB ID: 5My6, full sequence is in the Supplementary Material) and the non-targeting control sdAb R3B23 (16) were coupled to *p*-SCN-Bn-DOTA chelator and radiolabeled with ^{225}Ac as described elsewhere (10). Briefly, the desired activity (2.0-8.7 MBq) of ^{225}Ac was mixed with 0.8 M ammonium acetate (pH 5.0) and incubated with sdAb-DOTA (100-150 µg) for 90 min at 55°C. The mixture was cooled to room temperature, quenched with 50 mM DTPA and Chelex 100 (BioRad Laboratories) in order to complex free ^{225}Ac, followed by purification on a PD-10 column (GE Healthcare, Piscataway, NJ), collected in 0.9% NaCl containing 5 mg/mL L-ascorbic acid (pH 4-5, radical scavenger) and filtered through a 0.22 µm filter (Millex, Merck Millipore, Burlington, MA). Protein-associated radioactivity was determined using instant thin-layer chromatography (ITLC) on silica gel impregnated glass fiber sheets (Agilent Technologies, Santa Clara, CA) using 0.05 M citrate buffer at pH 4.0.

Cell lines and *in vitro* assays

SKOV-3 (ATCC Cat# HTB-77, RRID:CVCL_0532, HER2^{pos}) was purchased from the American Type Culture Collection (Manassas, VA) and HER2^{pos} SKOV-3-Luc-IP1 (SKOV3.IP1) cells were transfected to express the enzyme firefly luciferase (Fluc+). These cells were specifically generated for intraperitoneal growth (obtained as a gift from prof. Marc Bracke from Ghent University, Belgium) (17). Both cell lines were grown in McCoy's 5A supplemented with 10% fetal bovine serum, streptomycin (100 µg/mL) and penicillin (100 IU/mL), generating working cell banks of up to no more than passage 10. Working cell banks were stored in liquid nitrogen and, upon thaw, propagated for no more than 5 to 10 additional

Downloaded from http://aacrjournals.org/mct/article-pdf/doi/10.1158/1535-7163.MCT-21-1021/3208456/mct-21-1021.pdf by Instytut Marii Sklodowskiej-Curie Oddzial w. Gliwicach user on 10 October 2022

passages. Absence of *Mycoplasma* was confirmed (Venor GeM Classic kit, Minerva Biolabs) before start of *in vitro* experiments. Besides assessment of *Mycoplasma*, no cell line authentication was performed.

Binding affinity, specificity and internalization of [^{225}Ac]Ac-DOTA-sdAbs were determined as described previously (10,18). *In vitro* cytotoxicity tests, including clonogenic assay (19) and determination of DNA double-strand-breaks (DSBs) via γ-H2AX foci imaging, were performed on SKOV-3 cells and described more in detail in Supplementary Material.

Animal models

Female CRL:Nu-FoxN1^{nu} mice (Charles River Laboratories, RRID:IMSR_CRL:088) were inoculated subcutaneously (s.c.) in the neck with 10×10^6 SKOV-3 cells and grown until they reached about 100-250 mm^3 for biodistribution studies, and intraperitoneally (i.p.) with 0.25×10^6 SKOV-3.IP1 cells for the therapy study. Tumor growth was measured using caliper (s.c.) or bioluminescence imaging (i.p.) (Biospace Lab, Paris) after i.p. injection of 100 µL of D-Luciferin (Promega, Leiden, The Netherlands). Dose-escalation studies were performed in normal female C57Bl/6 mice (Charles River Laboratories, RRID:SCR_003792). All animal protocols were approved by the ethical committee of the Vrije Universiteit Brussel.

Biodistribution and organ-absorbed doses

Specificity of targeting was evaluated in mice bearing s.c. SKOV-3 xenografts (n = 3) of 100-250 mm^3. These tumor volumes were reached approximately 3 weeks after s.c. inoculation with 10×10^6 cells. Mice were injected intravenously (i.v.) with 20.5±2.2 kBq (2.5±0.3 µg) of [^{225}Ac]Ac-DOTA-2Rs15d either alone or in the presence of 50-molar excess of 2Rs15d to block HER2-receptors, or with 24.2±1.8 kBq (2.0±0.5 µg) of [^{225}Ac]Ac-DOTA-R3B23. Administrations were done in combination with 150 mg/kg of Gelofusine to reduce kidney uptake as described previously (10). Mice were euthanized 1 h post-injection (p.i.), after which major organs and tissues were isolated, weighed, and counted along with injected standards on the automatic gamma-counter (Cobra II 5003, Canberra Packard).

In parallel, mice (n = 3) were injected i.v. with 25.8±2.0 kBq (1.1±0.1 µg) [^{225}Ac]Ac-DOTA-2Rs15d together with 150 mg/kg of Gelofusine and euthanized at several time points starting

Downloaded from http://aacrjournals.org/mct/article-pdf/doi/10.1158/1535-7163.MCT-21-1021/3208456/mct-21-1021.pdf by Instytut Marii Sklodowskiej-Curie Oddzial w. Gliwicach user on 10 October 2022

from 1 h up to 168 h p.i., and processed as described above. The acquired uptake values, expressed as a percentage of injected activity per gram of tissue (% IA/g), were time-integrated to obtain the residence time per gram tissue by trapezoid integration method (13). The absorbed doses were calculated using S values for ^{225}Ac obtained from RADAR phantoms (www.doseinfo-radar.com/RADARphan.html). The S value for a 1 g sphere (4.40×10^{-9} J/kBq.s) was used to calculate all organ doses (14) and includes the energy deposition of all radioactive daughters of ^{225}Ac. The dosimetry calculation assumes that decay of all daughter radioisotopes occur in the same location as the parent radioisotope.

α-camera imaging

The ionizing-radiation quantum imaging detector (iQID) camera was used for high resolution *ex vivo* imaging (20). In brief, cryo-sections (10 μm) of tumors and kidneys of SKOV-3 xenografted mice co-injected with 150 mg/kg Gelofusine (n = 3/group) were transferred on a scintillation film (EJ-440; Eljen Technology, Sweetwater). SKOV-3 tumor-bearing mice (n = 3) received 120±0.4 kBq [^{225}Ac]Ac-DOTA-2Rs15d and were sacrificed after 1, 4 and 24 h. Images were rebinned by summing neighboring voxels to reduce the noise. The histogram and multi-term gaussian distributions were obtained through MATLAB R2020b (RRID:SCR_001622). Homogeneity of cryo-slices was quantitatively determined by the use of area under the curve (AUC) figure of merit analogous to the method described earlier (21).

Dose-escalation and therapeutic efficacy of [^{225}Ac]Ac-DOTA-2Rs15d

First, groups of normal female C57Bl/6 mice (n = 3) were i.v. injected with 19, 38 or 75 kBq of [^{225}Ac]Ac-DOTA-2Rs15d, or an equal volume of 0.9% NaCl with 5 mg/mL L-ascorbic acid and 150 mg/kg Gelofusine. Animals were weighed weekly and checked daily for general health and wellbeing. Mice were euthanized when one of the following endpoints were reached: (i) weight loss >20% of original body weight, (ii) physical appearance, (iii) animal behavior.

Next, mice with i.p. SKOV-3.IP1 tumor xenografts (n = 8) were injected with either (i) one dose (day 7 after tumor inoculation); or (ii) three consecutive doses (on day 7, 10, 14) of

Downloaded from http://aacrjournals.org/mct/article-pdf/doi/10.1158/1535-7163.MCT-21-1021/3208456/mct-21-1021.pdf by Instytut Marii Sklodowskiej-Curie Oddzial w. Gliwicach user on 10 October 2022

86.84±8.97 kBq [^{225}Ac]Ac-DOTA-2Rs15d (5.46±1.28 µg)*;* (iii) trastuzumab first at 7.5 mg/kg loading (190 µg) dose followed by two maintenance doses of 3.5 mg/kg (90 µg) to mimic patient treatment schemes (loading dose: day 7; maintenance dose: day 10, 14); (iv) a trastuzumab regimen as described in (iii) followed by three consecutive doses of 86.84±8.97 kBq [^{225}Ac]Ac-DOTA-2Rs15d (day 7, 10, 14); (v) three consecutive doses of 34.33±21.78 kBq [^{225}Ac]Ac-DOTA-R3B23 (6.67±2.31 µg) on day 7, 10, 14; or (vi) an equal volume of vehicle solution (0.9% NaCl + 5 mg/mL L-ascorbic acid) at identical time-points as the treated groups. All samples were co-injected with 150 mg/kg Gelofusine. Tumor development was measured over time using bioluminescence imaging. Dropouts were considered when one of the following endpoints was reached: (i) severe ascites, (ii) sudden >20% weight loss, (iii) physical appearance, (iv) animal behavior, (v) BLI signal exceeding 3×10^8 ph/s/cm^2/sr.

From all abovementioned treatment groups in both studies, various organs and tissues were isolated, fixed in formalin, and embedded in paraffin wax. Sections of 4 µm thickness were taken and stained with hematoxylin and eosin (H&E). The sections were examined by light microscopy by AnaPath Services GmbH (Liestal, Switzerland) for signs of toxicity.

Statistical analysis

All *in vitro* data are presented as mean ± standard deviation (SD) of at least three independent experiments. Differences in cytotoxicity or tissue uptake were tested with a one-tailed Student's *t*-test using GraphPad Prism 5.01 (RRID:SCR_002798). A *P*-value below 0.05 was considered statistically significant. Differences in mean survival from therapy studies were analyzed with the log-rank Mantel-Cox test.

Data availability statement

Data generated in this study are included in the article or uploaded as online Supplementary Material. The raw datasets used and/or analyzed during this study are available from the corresponding author upon reasonable request.

Downloaded from http://aacrjournals.org/mct/article-pdf/doi/10.1158/1535-7163.MCT-21-1021/3208456/mct-21-1021.pdf by Instytut Marii Sklodowskiej-Curie Oddzial w. Gliwicach user on 10 October 2022

Results

Radiolabeling and *in vitro* evaluation of [^{225}Ac]Ac-DOTA-sdAbs

Mass spectrometry revealed successful *p*-SCN-Bn-DOTA conjugation with an average of one or two chelators per sdAb (Supplementary Fig. S1). The radiolabeling yield was >90% (n = 21) for all bioconjugates labeled with ^{225}Ac (2.0-8.7 MBq) after 90 min incubation at 55°C, and the radiochemical purity was >98% (n = 21) after purification on PD-10 as determined by ITLC. The specific activity of all radiolabeled compounds was 105-678 kBq/nmol.

Binding of [^{225}Ac]Ac-DOTA-2Rs15d to HER2-receptor was specific (P< 0.001) as it could be blocked by an excess of unlabeled 2Rs15d, whereas binding of [^{225}Ac]Ac-DOTA-R3B23 was negligible (Supplementary Fig. S2A). The determined K_D=3.50±0.17 nM for [^{225}Ac]Ac-DOTA-2Rs15d revealed high affinity towards HER2-receptor (Supplementary Fig. S2B). The level of receptor-mediated internalization measured 36.03±1.73% after 1 h and dropped to 14.83±0.54% at 24 h (Supplementary Fig. S2C).

The number of colonies decreased with increasing amounts of radioactivity (**Fig. 1A**). At low radioactivity (0.1-0.8 kBq/mL) the surviving fractions (SFs) were approximately 100% with no significant difference between [^{225}Ac]Ac-DOTA-2Rs15d and the control groups (P >0.42) (Supplementary Fig. S3). The increased activity of [^{225}Ac]Ac-DOTA-2Rs15d reduced SFs to 75.2±6.1% and 3.4±0.7% at 1.0 and 60.0 kBq/mL, respectively, while in the presence of an excess of unlabeled 2Rs15d the SFs measured 95.9±2.7% and 8.2±0.7%, which was significantly higher (P <0.004). Cells treated with non-targeting [^{225}Ac]Ac-DOTA-R3B23 resulted in SFs of 87.1±6.8% and 13.6±0.9% at 1.0 and 60.0 kBq/mL, respectively (P <0.002). In case of the highest applied radioactivity (120 kBq/mL), the resulting number of colonies was too low to observe a statistical difference between all treated groups. The calculated EC_{50} values for the respective treatment groups were 3.9±1.1 kBq/mL for [^{225}Ac]Ac-DOTA-2Rs15d alone, 7.4±1.1 kBq/mL when co-incubated with an excess of unlabeled 2Rs15d, and 11.3±1.1 kBq/mL for [^{225}Ac]Ac-DOTA-R3B23. The determined D_0 values were: 20.0±2.4 kBq/mL, 24.2±2.2 kBq/mL and 31.7±2.4 kBq/mL for [^{225}Ac]Ac-DOTA-

Downloaded from http://aacrjournals.org/mct/article-pdf/doi/10.1158/1535-7163.MCT-21-1021/3208456/mct-21-1021.pdf by Instytut Marii Sklodowskiej-Curie Oddzial w. Gliwicach user on 10 October 2022

2Rs15d alone, blocked with an excess of unlabeled 2Rs15d and [^{225}Ac]Ac-DOTA-R3B23, respectively (**Fig. 1B**).

The number of spontaneous DNA DSBs in non-treated (NT) SKOV-3 cells was 18.9±3.1 per cell, whereas in cells exposed to [^{225}Ac]Ac-DOTA-2Rs15d this number varied in a dose-dependent manner (**Fig. 1C** and **D**) with values of 32.6±4.3, 45.5±7.7 and 78.8±4.9 ($P< 0.03$) after treatment with 15, 125 and 625 kBq/mL, respectively. In case of the two lower radioactive concentrations the average number of DNA DSBs was higher than values obtained for cells incubated with an excess of unlabeled 2Rs15d or non-targeting [^{225}Ac]Ac-DOTA-R3B23, however not significantly different (P=0.215) (**Fig. 1C** and **D**).

Biodistribution and dose-escalation of [^{225}Ac]Ac-DOTA-sdAbs

As presented in **Fig. 2A**, the accumulation of [^{225}Ac]Ac-DOTA-2Rs15d in SKOV-3 tumors was specific and measured 7.49±0.74% IA/g at 1 h p.i., which was significantly higher than what was measured for [^{225}Ac]Ac-DOTA-2Rs15d co-administered with excess of unlabeled 2Rs15d (2.31±0.06% IA/g; P <0.00015), or for [^{225}Ac]Ac-DOTA-R3B23 (0.25±0.09% IA/g; P<0.00004).

The time-dependent biodistribution of [^{225}Ac]Ac-DOTA-2Rs15d in SKOV-3 tumor xenografted mice is presented in **Fig. 2B** and **Table 1**. The high tumor uptake was observed already after 1 h p.i. with a value of 8.36±0.23% IA/g, increasing to 9.64±1.69% IA/g at 3 h followed by a decrease to 2.24±1.00% IA/g after 168 h. In kidneys, 8.98±3.30% IA/g was measured at 1 h, which decreased to 1.91±1.15% IA/g at 168 h. Liver and bone uptake were very low at all-time points, indicating no substantial loss of ^{225}Ac. Radioactivity concentration in other tissues was low always (< 0.85% IA/g). Tumor-to-liver ratios increased from 12.62±0.73 at 1 h to 33.40±12.13 at 6 h and later dropped to 5.60±0.66 at 168 h (**Table 1**), while tumor-to-kidney ratios increased from 1.03±0.42 at 1 h to 1.55±0.24 at 96 h, respectively. Organ-absorbed doses were calculated for 1 kBq of [^{225}Ac]Ac-DOTA-2Rs15d and are summarized in **Table 1**. The highest absorbed dose was delivered to tumor (115.58 mGy/kBq), while kidneys received 103.50 mGy/kBq. Doses delivered to other healthy organs and tissues were very low.

Downloaded from http://aacrjournals.org/mct/article-pdf/doi/10.1158/1535-7163.MCT-21-1021/3208456/mct-21-1021.pdf by Instytut Marii Sklodowskiej-Curie Oddzial w. Gliwicach user on 10 October 2022

In a dose-escalation study, groups of normal female C57Bl/6 mice received a single administration of increasing radioactive amounts of [^{225}Ac]Ac-DOTA-2Rs15d ranging 19–75 kBq or non-radioactive vehicle solution (control). All animals in the control group were included until the end of the study (200 days) and sacrificed at the end. In that case the mean survival was considered undefined. Animal groups that received 75 and 38 kBq counted for a mean survival of 166 and 145 days respectively (P = 0.277) (**Fig. 2C**). Weight progression during dose escalation study of [^{225}Ac]Ac-DOTA-2Rs15d in healthy C57Bl/6 mice is presented in **Fig. 2D**. Histopathological analysis resulted in mild to serious tubulopathy in mice receiving [^{225}Ac]Ac-DOTA-2Rs15d **(Fig. 2E** and **F, Table 2).**

Digital autoradiography of tumors and kidneys was used to evaluate distribution of radioactivity after injection of [^{225}Ac]Ac-DOTA-2Rs15d with co-infusion of Gelofusine at 1, 4 and 24 h (**Fig. 3**). A clear intratumoral distribution was observed already 1 h p.i. and was maintained until 24 h (**Fig. 3A**). In kidneys, α-imaging at 1, 4 and 24 h revealed marked differences in intrarenal activity distribution (**Fig. 3B**). At 1 h, high-intensity areas of activity were observed in the cortical region, decreasing over time indicating efficient clearance of [^{225}Ac]Ac-DOTA-2Rs15d. **Fig. 3C** presents a quantitative analysis of the activity distribution from the kidney 4 h p.i. depicted in **Fig. 3B**. The extracted histogram shows a non-uniform uptake. Multi-term gaussian distributions were fitted to the histogram data of cortex ROI. From **Fig. 3D** a wash-out over time can be observed. Homogeneity was assessed by plots where the total signal fraction is displayed as a function of the total area fraction. A completely uniform ROI corresponds to a linear function and an AUC of 0.5. Both cortex ROIs (**Fig. 3E**) as well as ROIs encompassing the whole tumor slice (**Fig. 3F**) show uniform activity distributions - cortex: 0.6186 (1h), 0.6042 (4h), 0.6274 (24h); and tumors: 0.6754 (1h), 0.6477 (4h), 0.6092 (24h).

Therapeutic efficacy of [^{225}Ac]Ac-DOTA-2Rs15d

The therapeutic efficacy study scheme is presented in **Fig. 4A**. Both a single and three consecutive administrations of [^{225}Ac]Ac-DOTA-2Rs15d resulted in a significantly longer mean survival of 101 and 143 days respectively, versus 56 days for mice receiving vehicle

Downloaded from http://aacrjournals.org/mct/article-pdf/doi/10.1158/1535-7163.MCT-21-1021/3208456/mct-21-1021.pdf by Instytut Marii Sklodowskiej-Curie Oddzial w. Gliwicach user on 10 October 2022

solution (P <0.0001) (**Fig. 4B**). No significant difference (P = 0.2151) in survival was observed between negative control groups receiving vehicle (56 days) or [^{225}Ac]Ac-DOTA-R3B23 (61 days). No significant difference in mean survival was observed between the trastuzumab regimen (100 days) and a single administration of [^{225}Ac]Ac-DOTA-2Rs15d (101 days; P = 1.000), while three consecutive doses of [^{225}Ac]Ac-DOTA-2Rs15d (143 days) increased the mean survival compared to the group receiving trastuzumab regimen or a single dose of [^{225}Ac]Ac-DOTA-2Rs15d (P <0.0389). Trastuzumab regimen alone led to a mean survival of 100 days, while trastuzumab regimen together with three consecutive injections of [^{225}Ac]Ac-DOTA-2Rs15d as an add-on therapy increased mean survival to 161 days; however, not significantly different from each other (P = 0.0558). These results are confirmed by a more stable weight, indicating less tumor progression for all mice treated with three repeated doses of [^{225}Ac]Ac-DOTA-2Rs15d alone or together with trastuzumab (**Fig. 4C**). The calculated absorbed dose for single 85 kBq and the cumulative therapeutic activity 255 kBq (3×85 kBq) of [^{225}Ac]Ac-DOTA-2Rs15d is about 9.8 Gy and 29.5 Gy in tumor, whereas in kidneys is 8.8 and 26.4 Gy, respectively (**Fig. 4D**).

The anti-tumor effect of [^{225}Ac]Ac-DOTA-2Rs15d was confirmed through bioluminescence imaging (Supplementary Fig. S4). Disease progression was retarded for animal groups treated with trastuzumab or [^{225}Ac]Ac-DOTA-2Rs15d compared to control groups. Mice which received repeated injections of [^{225}Ac]Ac-DOTA-2Rs15d alone or in combination with trastuzumab revealed a complete absence of BLI signal over time. However, histopathological evaluation of kidneys revealed a number of substantial inflammatory lesions consisting of tubular dilation in mice receiving a single (85 kBq) and triple dose (3×85 kBq = 255 kBq) of [^{225}Ac]Ac-DOTA-2Rs15d, while this was not observed in animals that received vehicle solution (**Fig. 4E-G**).

Discussion

In this study, we report a complete *in vitro* and *in vivo* evaluation of the HER2-targeting sdAb 2Rs15d radiolabeled with the α-particle emitter ^{225}Ac. 2Rs15d has been evaluated previously

Downloaded from http://aacrjournals.org/mct/article-pdf/doi/10.1158/1535-7163.MCT-21-1021/3208456/mct-21-1021.pdf by Instytut Marii Sklodowskiej-Curie Oddzial w. Gliwicach user on 10 October 2022

as a vector for both imaging (22–25) and targeted radionuclide therapy (TRNT) (13,14,26), and is characterized by high binding specificity and affinity to HER2-receptor, and high tumor-to-background ratios *in vivo*. Fast clearance from blood allows repeated administration, though, with a risk of inducing long-term toxicity to kidneys. Indeed, depending on the radionuclide used, fast clearance of radiolabeled sdAb can result in significant accumulation and retention of radioactivity in kidneys. However, radioactive dose fractionation has already indicated in the clinic that it can reduce toxicity to critical organs and tissues in patients with multi-resistant neuroendocrine tumors (3) as this strategy allows time for healthy tissue regeneration. Results of preclinical therapy studies with ^{225}Ac-labeled trastuzumab (27) also suggest that fractionation is more effective particularly in treatment of larger metastatic-clusters, as it avoids early mortality which is seen when administering single high radioactive dose.

A few preclinical studies have described HER2-sdAb-based TRNT using α-particle emitting radionuclides (11,14,28). We recently reported therapeutic efficacy [^{225}Ac]Ac-DOTA-2Rs15d in mice with intracranial HER2^{pos} tumor xenografts (14). The combination of trastuzumab and [^{225}Ac]Ac-DOTA-2Rs15d resulted in a significant increase in survival compared to control groups. In addition, [^{213}Bi]Bi-DTPA-2Rs15d revealed to be promising with confirmed therapeutic efficacy in mice bearing intraperitoneal HER2^{pos} tumor xenografts (28). Nonetheless, *in vivo* TAT appeared to be challenging due to the very short half-life of ^{213}Bi and resulted in a therapeutic index below 0.5. MAbs (e.g. lintuzumab) radiolabeled with ^{213}Bi and ^{225}Ac were evaluated for various types of cancer (29,30); however, accumulation of cytotoxic radiation in critical organs such as liver and bone-marrow remains a major dose-limiting factor for mAbs. The recent clinical successes using ^{225}Ac-labeled peptides such as PSMA-617, Substance P and Octreotide have shown their potential in TAT (5,31,32). In this study, we further investigated the use of [^{225}Ac]Ac-DOTA-2Rs15d to treat intraperitoneal metastatic disease in mice.

[^{225}Ac]Ac-DOTA-2Rs15d was obtained with high radiochemical yield and specific activity. Addition of DTPA and Chelex 100 prior to purification improved the radiochemical purity of a

Downloaded from http://aacrjournals.org/mct/article-pdf/doi/10.1158/1535-7163.MCT-21-1021/3208456/mct-21-1021.pdf by Instytut Marii Sklodowskiej-Curie Oddzial w. Gliwicach user on 10 October 2022

final product compared to what was reported before (10). [^{225}Ac]Ac-DOTA-2Rs15d bound HER2-receptor specifically both *in vitro* and *in vivo*, and targeting capacity was not affected by conjugation of two chelators per one sdAb. The level of receptor-mediated internalization of [^{225}Ac]Ac-DOTA-2Rs15d was higher compared to 2Rs15d radiolabeled with ^{211}At via [^{211}At]At-SGMAB (*ca*. 15% at 1-24 h), [^{211}At]At-SAB (*ca*. 25% at 1 h and 15% at 24 h) and [^{211}At]At-MSB (*ca*. 25% at 1 h and 20% at 24 h) or with ^{131}I through [^{131}I]I-SGMIB (9.13±2.37% at 1 h and 14.39±1.95% at 24 h) prosthetic groups, respectively (11,26). This is an important result taking into account a serial decay of ^{225}Ac into radioactive daughters, since better internalization prevents the escape of those radionuclides from cancerous cells, which may result in an increased therapeutic efficacy and lower toxicity (33,34). Higher internalization levels were observed previously for mAbs labeled with radiometals compared to radiohalogens. A potential explanation could be the increased intracellular retention of catabolic products containing radiometals, perhaps within lysosomes (35). The level of internalization obtained in this study for [^{225}Ac]Ac-DOTA-2Rs15d seems higher than what was observed for the same sdAb labeled with radiohalogens. However, we have to keep in mind that different radiolabeling methods were used, including one- or two-steps procedures as for ^{211}At (11). In addition, the results for [^{131}I]I-SGMIB-2Rs15d were obtained using a different cell line, BT474/M1 (26).

[^{225}Ac]Ac-DOTA-2Rs15d was toxic to HER2^{pos} SKOV-3 cells, with an EC_{50} value of 3.9±1.1 kBq/mL which was lower compared to the value obtained via the MTS assay (10.2±1.2 kBq/mL) (10). The clonogenic assay, performed in the current study, is considered to be more reliable as it reveals the actual number of cells that survived treatment and can further proliferate to form colonies, whereas the MTS measures the cell metabolism and does not differentiate between cells in early or late stage apoptosis. *In vitro* cytotoxic effect of [^{225}Ac]Ac-DOTA-2Rs15d was further supported by its ability to induce irreparable DSBs in DNA. However, further assay optimization (e.g. incubation time) is still required since major differences between [^{225}Ac]Ac-DOTA-2Rs15d and the controls were not observed. *In vivo*, [^{225}Ac]Ac-DOTA-2Rs15d accumulated rapidly in tumor, with high uptake measured as early

Downloaded from http://aacrjournals.org/mct/article-pdf/doi/10.1158/1535-7163.MCT-21-1021/3208456/mct-21-1021.pdf by Instytut Marii Sklodowskiej-Curie Oddzial w. Gliwicach user on 10 October 2022

as 1 h p.i.. After 168 h (7 d), a significant amount of radioactivity was still retained in tumor. Accumulation in normal organs and tissues was low at all time-points, except in kidneys. The observed tumor uptake corresponds well to what was previously obtained with 2Rs15d radiolabeled with ^{211}At, ^{177}Lu, ^{18}F or ^{213}Bi when administered to the same mouse model (11,13,23,28). We previously observed elevated liver uptake upon i.v. administration of [^{225}Ac]Ac-DOTA-2Rs15d, probably due to non-specific binding of ^{225}Ac to the protein and not through stable DOTA chelator complexation. It is known that non-complexed ^{225}Ac highly accumulates in liver (10). Addition of an excess of DTPA to the reaction mixture right after ^{225}Ac-complexation was described to result in reduced retention in liver (14). Therefore, in the current manuscript, an excess of DTPA together with cationic Chelex resin was added to the reaction mixture prior to purification of [^{225}Ac]Ac-DOTA-2Rs15d, and successfully avoided retention of radioactivity in liver.

The clearance pattern in kidneys was in line with what has been observed previously for [^{177}Lu]Lu-DOTA-2Rs15d (13) and about twice lower to that measured for [^{213}Bi]Bi-DTPA-2Rs15d (28). All radiolabeled sdAbs were co-injected with 150 mg/kg Gelofusine which is described to reduce the kidney retention with 40-50% (10,13,14). The different physiochemical properties of radiolabeled sdAbs either with *p*-SCN-Bn-CHX-A”-DTPA or *p*-SCN-Bn-DOTA as chelating moieties might influence the stability of formed complexes and the extent of renal accumulation. Dosimetry estimations for [^{225}Ac]Ac-DOTA-2Rs15d resulted in a therapeutic index of 1.0 compared to a therapeutic index of 0.16 for [^{213}Bi]Bi-DTPA-2Rs15d (28). An explanation for this observation might be the higher uptake in kidneys of [^{213}Bi]Bi-DTPA-2Rs15d together with the high dose rate of the latter radioisotope, which might increase the risk of inducing acute toxicity within cortical compartment of kidneys.

Therapeutic efficacy study in athymic nude mice was designed in such a way to understand the therapeutic potential, even though we assumed that the chosen doses could cause late stage toxicity, especially in kidneys. As a result, a single radioactive dose of 85 kBq [^{225}Ac]Ac-DOTA-2Rs15d was selected based on the insights from dose-escalation study. For this activity an absorbed dose in kidneys is 8.8 Gy, whereas in case of a cumulative

Downloaded from http://aacrjournals.org/mct/article-pdf/doi/10.1158/1535-7163.MCT-21-1021/3208456/mct-21-1021.pdf by Instytut Marii Sklodowskiej-Curie Oddzial w. Gliwicach user on 10 October 2022

therapeutic activity of 255 kBq (3×85 kBq) [^{225}Ac]Ac-DOTA-2Rs15d is about 26.4 Gy, which remains close to the renal toxicity threshold of 23 Gy. However, any reference to this limit should be done with care, as it was determined via external beam irradiation and assumes homogenous radiation distribution in kidneys, which is not representative in case of short-range radiation of high LET α-particles emitted from radionuclides accumulated in tissue (36). Moreover, α-camera imaging confirmed that radioactivity distribution in kidneys was heterogeneous and appeared to be concentrated in the cortical compartment of kidneys. Therefore, a mean absorbed dose to a whole organ seems not sufficient to accurately assess dose limits on an organ and sub-organ level. In addition, when considering α-particle radiation one should take into account the relative biological effectiveness (RBE) to enable comparability between doses from different radiation types. An RBE value of 5 is often used for studies with ^{225}Ac (3,4) which always results in a higher RBE-weighted absorbed doses to organs and tissues. As a result the calculated RBE-weighed absorbed doses to kidneys for a single administration (85 kBq) and three consecutive administrations are 44 Gy and 132 Gy, respectively. However, the latter dose is an extrapolation done for a single injection of 255 kBq of [^{225}Ac]Ac-DOTA-2Rs15d, while it was administered in a fractionated regimen for therapy.

The high absorbed dose to tumor in case of [^{225}Ac]Ac-DOTA-2Rs15d and the resulting positive impact on survival indicates increased potency of α-particle radiation over more conventional β^--particle radiation. Indeed, administration of 46.25 MBq of ^{131}I-labeled 2Rs15d resulted in an absorbed dose to tumor of about 15 Gy and 10 Gy to kidneys and led to a mean survival of about 59 days in the same tumor-xenografted mouse model (26). Repeated [^{225}Ac]Ac-DOTA-2Rs15d injections combined with trastuzumab further increased the mean survival in comparison to trastuzumab regimen alone, which indicates the potential of ^{225}Ac-labeled 2Rs15d as an add-on therapy to trastuzumab. Importantly, 2Rs15d binds domain I of the HER2-receptor, whereas trastuzumab binds domain IV, so no binding competition exists between both targeting moieties (24,26). Therefore, [^{225}Ac]Ac-DOTA-2Rs15d might be also considered as a therapeutic strategy in particular occasions where patients show resistance

Downloaded from http://aacrjournals.org/mct/article-pdf/doi/10.1158/1535-7163.MCT-21-1021/3208456/mct-21-1021.pdf by Instytut Marii Sklodowskiej-Curie Oddzial w. Gliwicach user on 10 October 2022

to treatment with trastuzumab or acquired resistance during therapy with final relapse and disease progression. Moreover, [^{225}Ac]Ac-DOTA-2Rs15d might be applied in cases where full intact monoclonal antibodies, like trastuzumab are not effective, for example in HER2^{pos} brain lesions (14). Despite very convincing therapeutic efficacy results presented in this study, there is also an indication of renal toxicity at high radioactive doses. Small radiolabeled peptides and proteins, such as [^{225}Ac]Ac-DOTA-2Rs15d, are characterized by fast blood clearance and in a few cases these are subsequently retained in kidneys. More so, ^{213}Bi which originates from the decay of ^{225}Ac accumulates in kidneys as well (33). Both pose concerns towards off-target toxicity. In case of ^{213}Bi, the chelation of free radiometal, competitive metal blockade, or the acceleration of renal clearance can reduce the accumulation of ^{225}Ac daughters in kidneys (34). So far, clinical cases describing peptide-based TAT using ^{225}Ac revealed no acute or sub-acute renal toxicity (32). Although, not obtained in randomized clinical trials, these early results indicate that the toxicity profile in a clinical setting is not yet fully understood and that the herein presented preclinical results should be interpreted with care. Nevertheless, high kidney uptake of [^{225}Ac]Ac-DOTA-2Rs15d underlines the need for thorough dose-reduction studies to identify the ideal dose and fractionation scheme to achieve treatment efficacy while keeping toxicity to kidneys minimal. In addition, it is worthwhile investigating how to further reduce the retention of radioactivity in kidneys. One possible strategy is the introduction of amino-acid-linkers between the sdAb and chelator complex (37–40) that are designed to be cleaved at the proximal tubular brush border membrane. This might allow radiometal complex to be separated from targeting moiety prior to interaction with lumen of the renal tubules, and therefore efficiently excreted into urine. Alternatively, positively charged amino acids (L-lysine or L-arginine) either separately or as a cocktail will be used in future studies to effectively reduce kidney retention as previously shown in both preclinical (41) and clinical studies in patients injected with [^{177}Lu]Lu-DOTA-TATE, where renal toxicity was significantly reduced with positively charged amino acids (42).

The present study demonstrates effective treatment of intraperitoneal disseminated tumors

Downloaded from http://aacrjournals.org/mct/article-pdf/doi/10.1158/1535-7163.MCT-21-1021/3208456/mct-21-1021.pdf by Instytut Marii Sklodowskiej-Curie Oddzial w. Gliwicach user on 10 October 2022

using [^{225}Ac]Ac-DOTA-2Rs15d, both alone as a single treatment as well as in combination with the HER2-targeting mAb trastuzumab. [^{225}Ac]Ac-DOTA-2Rs15d holds promise for further investigation; however, a better understanding of dose-response and dose-toxicity relationships are needed. With the recent successful introduction of ^{225}Ac-labeled peptides in the clinic, sdAb-based TAT might also find its way towards clinical translation.

Authors' Contributions

M. Rodak: Methodology, formal analysis, investigation, data curation, writing – original draft, visualization. **Y. Dekempeneer:** Methodology, formal analysis, investigation, data curation, writing – original draft, visualization. **M. Wojewódzka:** Methodology, formal analysis. **V. Caveliers:** Methodology, resources. **P. Covens:** Methodology, data curation. **B.W. Miller:** Methodology, resources. **M.B. Sevenois:** Methodology, formal analysis, data curation. **F. Bruchertseifer:** Methodology, resources. **A. Morgenstern:** Methodology, resources. **T. Lahoutte:** Methodology, resources. **M. D'Huyvetter:** Conceptualization, methodology, investigation, writing – review and editing, supervision, project administration, funding acquisition. **M. Pruszyński:** Conceptualization, methodology, investigation, writing – review and editing, supervision, project administration, funding acquisition.

Acknowledgments

This study was supported by grant funding from the National Science Centre, Poland (SONATA-BIS9 research project 2019/34/E/ST4/00080) and supported by bilateral cooperation between Research Foundation-Flanders (FWO) and Polish Academy of Sciences (PAS). T. Lahoutte is Senior Clinical Investigator and M. D'Huyvetter is postdoctoral fellow of the FWO. M. Rodak was funded by Operational Project Knowledge Education Development, co-financed by the European Social Fund (POWR.03.02.00-00-I009/17-00).

References

1. Bruchertseifer F, Kellerbauer A, Malmbeck R, Morgenstern A. Targeted alpha therapy with bismuth-213 and actinium-225: Meeting future demand. J Labelled Comp Radiopharm. 2019;62:794–802.

Downloaded from http://aacrjournals.org/mct/article-pdf/doi/10.1158/1535-7163.MCT-21-1021/3208456/mct-21-1021.pdf by Instytut Marii Sklodowskiej-Curie Oddzial w. Gliwicach user on 10 October 2022

2. Poty S, Francesconi LC, McDevitt MR, Morris MJ, Lewis JS. α-Emitters for radiotherapy: from basic radiochemistry to clinical studies-part 2. J Nucl Med. 2018;59:1020–7.
3. Kratochwil C, Bruchertseifer F, Giesel F, Apostolidis C, Haberkorn U, Morgenstern A. Ac-225-DOTATOC - an empiric dose finding for alpha particle emitter based radionuclide therapy of neuroendocrine tumors. J Nucl Med. 2015;56(3 suppl):1232.
4. Kratochwil C, Bruchertseifer F, Rathke H, Bronzel M, Apostolidis C, Weichert W, et al. Targeted α-therapy of metastatic castration-resistant prostate cancer with ^{225}Ac-PSMA-617: dosimetry estimate and empiric dose finding. J Nucl Med. 2017;58:1624–31.
5. Kratochwil C, Bruchertseifer F, Giesel FL, Weis M, Verburg FA, Mottaghy F, et al. ^{225}Ac-PSMA-617 for PSMA-targeted α-radiation therapy of metastatic castration-resistant prostate cancer. J Nucl Med. 2016;57:1941–4.
6. Haberkorn U, Giesel F, Morgenstern A, Kratochwil C. The future of radioligand therapy: α, β, or both? J Nucl Med. 2017;58:1017–8.
7. Tagawa ST, Sun M, Sartor AO, Thomas C, Singh S, Bissassar M, et al. Phase I study of ^{225}Ac-J591 for men with metastatic castration-resistant prostate cancer (mCRPC). J Clin Oncol. 2021;39(15 suppl):5015.
8. Atallah EL, Orozco JJ, Craig M, Levy MY, Finn LE, Khan SS, et al. A phase 2 study of Actinium-225 (^{225}Ac)-lintuzumab in older patients with untreated acute myeloid leukemia (AML) - Interi analysis of 1.5 μCi/kg/dose. Blood. 2018;132(1 suppl):1457.
9. Dekempeneer Y, Keyaerts M, Krasniqi A, Puttemans J, Muyldermans S, Lahoutte T, et al. Targeted alpha therapy using short-lived alpha-particles and the promise of nanobodies as targeting vehicle. Expert Opin Biol Ther 2016;16:1035–47.
10. Pruszynski M, D'Huyvetter M, Bruchertseifer F, Morgenstern A, Lahoutte T. Evaluation of an anti-HER2 nanobody labeled with ^{225}Ac for targeted α-particle therapy of cancer. Mol Pharm. 2018;15:1457–66.

Downloaded from http://aacrjournals.org/mct/article-pdf/doi/10.1158/1535-7163.MCT-21-1021/3208456/mct-21-1021.pdf by Instytut Marii Sklodowskiej-Curie Oddzial w. Gliwicach user on 10 October 2022

11. Dekempeneer Y, Bäck T, Aneheim E, Jensen H, Puttemans J, Xavier C, et al. Labeling of anti-HER2 nanobodies with Astatine-211: optimization and the effect of different coupling reagents on their *in vivo* behavior. Mol Pharm. 2019;16:3524–33.
12. Nonnekens J, Chatalic KLS, Molkenboer-Kuenen JDM, Beerens CEMT, Bruchertseifer F, Morgenstern A, et al. ^{213}Bi-Labeled prostate-specific membrane antigen-targeting agents induce DNA double-strand breaks in prostate cancer xenografts. Cancer Biother Radiopharm. 2017;32:67–73.
13. D'Huyvetter M, Vincke C, Xavier C, Aerts A, Impens N, Baatout S, et al. Targeted radionuclide therapy with a ^{177}Lu-labeled anti-HER2 nanobody. Theranostics. 2014;4:708–20.
14. Puttemans J, Dekempeneer Y, Eersels JL, Hanssens H, Debie P, Keyaerts M, et al. Preclinical targeted α- and β$^-$-radionuclide therapy in HER2-positive brain metastasis using camelid single-domain antibodies. Cancers. 2020;12:1017.
15. Zielinska B, Apostolidis C, Bruchertseifer F, Morgenstern A. An improved method for the production of Ac-225/Bi-213 from Th-229 for targeted alpha therapy. Solvent Extr Ion Exch. 2007;25:339–49.
16. Lemaire M, D'Huyvetter M, Lahoutte T, Van Valckenborgh E, Menu E, De Bruyne E, et al. Imaging and radioimmunotherapy of multiple myeloma with anti-idiotypic Nanobodies. Leukemia. 2014;28:444–7.
17. De Vlieghere E, Carlier C, Ceelen W, Bracke M, De Wever O. Data on *in vivo* selection of SK-OV-3 Luc ovarian cancer cells and intraperitoneal tumor formation with low inoculation numbers. Data Brief. 2016;6:542–9.
18. Pruszynski M, Koumarianou E, Vaidyanathan G, Revets H, Devoogdt N, Lahoutte T, et al. Improved tumor targeting of anti-HER2 nanobody through N-succinimidyl 4-guanidinomethyl-3-iodobenzoate radiolabeling. J Nucl Med. 2014;55:650–6.
19. Franken NAP, Rodermond HM, Stap J, Haveman J, van Bree C. Clonogenic assay of cells *in vitro*. Nat Protoc. 2006;1:2315–9.

Downloaded from http://aacrjournals.org/mct/article-pdf/doi/10.1158/1535-7163.MCT-21-1021/3208456/mct-21-1021.pdf by Instytut Marii Sklodowskiej-Curie Oddzial w. Gliwicach user on 10 October 2022

20. Miller BW, Frost SHL, Frayo SL, Kenoyer AL, Santos E, Jones JC, et al. Quantitative single-particle digital autoradiography with α -particle emitters for targeted radionuclide therapy using the iQID camera. Med Phys. 2015;42:4094–105.

21. Miller BW, Bowen JM, Morrison EC. High-resolution, single-particle digital autoradiography of actinide sources using microcapillary array collimators and the iQID camera. Appl Radiat Isot. 2020;166:109348.

22. Xavier C, Vaneycken I, D'Huyvetter M, Heemskerk J, Keyaerts M, Vincke C, et al. Synthesis, precilinical validation, dosimetry, and toxicity of [^{68}Ga]Ga-NOTA-anti-HER2 nanobodies for iPET imaging of HER2 receptor expression in cancer. J Nucl Med. 2013;54:776–84.

23. Xavier C, Blykers A, Vaneycken I, D'Huyvetter M, Heemskerk J, Lahoutte T, et al. ^{18}F-nanobody for PET imaging of HER2 overexpressing tumors. Nucl Med Biol. 2016;43:247–52.

24. Vaneycken I, Devoogdt N, Van Gassen N, Vincke C, Xavier C, Wernery U, et al. Preclinical screening of anti-HER2 nanobodies for molecular imaging of breast cancer. FASEB J. 2011;25:2433–46.

25. Massa S, Xavier C, De Vos J, Caveliers V, Lahoutte T, Muyldermans S, et al. Site-specific labeling of cysteine-tagged camelid single-domain antibody-fragments for use in molecular imaging. Bioconjug Chem. 2014;25:979–88.

26. D'Huyvetter M, De Vos J, Xavier C, Pruszynski M, Sterckx YGJ, Massa S, et al. ^{131}I-labeled anti-HER2 camelid sdAb as a theranostic tool in cancer treatment. Clin Cancer Res. 2017;23:6616–28.

27. Borchardt PE, Yuan RR, Miederer M, McDevitt MR, Scheinberg DA. Targeted actinium-225 *in vivo* generators for therapy of ovarian cancer. Cancer Res. 2003;63:5084–90.

28. Dekempeneer Y, Caveliers V, Ooms M, Maertens D, Gysemans M, Lahoutte T, et al. Therapeutic efficacy of ^{213}Bi-labeled sdAbs in a preclinical model of ovarian cancer. Mol Pharm. 2020;17:3553–66.

Downloaded from http://aacrjournals.org/mct/article-pdf/doi/10.1158/1535-7163.MCT-21-1021/3208456/mct-21-1021.pdf by Instytut Marii Sklodowskiej-Curie Oddzial w. Gliwicach user on 10 October 2022

29. McDevitt MR, Finn RD, Ma D, Larson SM, Scheinberg DA. Preparation of alpha-emitting ^{213}Bi-labeled antibody constructs for clinical use. J Nucl Med. 1999;40:1722–7.

30. Miederer M, McDevitt MR, Sgouros G, Kramer K, Cheung NK, Scheinberg DA. Pharmacokinetics, dosimetry, and toxicity of the targetable atomic generator, ^{225}Ac-HuM195, in nonhuman primates. J Nucl Med. 2004;45:129–37.

31. Królicki L, Bruchertseifer F, Kunikowska J, Koziara H, Pawlak D, Kuliński R, et al. Dose escalation study of targeted alpha therapy with [^{225}Ac]Ac-DOTA-substance P in recurrence glioblastoma – safety and efficacy. Eur J Nucl Med Mol Imaging. 2021;48:3595–605.

32. Kratochwil C, Apostolidis L, Rathke H, Apostolidis C, Bicu F, Bruchertseifer F, et al. Dosing ^{225}Ac-DOTATOC in patients with somatostatin-receptor-positive solid tumors: 5-year follow-up of hematological and renal toxicity. Eur J Nucl Med Mol Imaging.

33. Schwartz J, Jaggi JS, O'Donoghue JA, Ruan S, McDevitt M, Larson SM, et al. Renal uptake of bismuth-213 and its contribution to kidney radiation dose following administration of actinium-225-labeled antibody. Phys Med Biol. 2011;56:721–33.

34. Jaggi JS, Kappel BJ, McDevitt MR, Sgouros G, Flombaum CD, Cabassa C, et al. Efforts to control the errant products of a targeted *in vivo* generator. Cancer Res. 2005;65:4888–95.

35. Shih LB, Thorpe SR, Griffiths GL, Diril H, Ong GL, Hansen HJ, et al. The processing and fate of antibodies and their radiolabels bound to the surface of tumor cells *in vitro*: a comparison of nine radiolabels. J Nucl Med. 1994;35:899–908.

36. Emami B, Lyman J, Brown A, Coia L, Goitein M, Munzenrider JE, et al. Tolerance of normal tissue to therapeutic irradiation. Int J Radiat Oncol Biol Phys. 1991;21:109–22.

37. Uehara T, Yokoyama M, Suzuki H, Hanaoka H, Arano Y. A Gallium-67/68–labeled antibody fragment for immuno-SPECT/PET shows low renal radioactivity without loss of tumor uptake. Clin Cancer Res. 2018;24:3309–16.

Downloaded from http://aacrjournals.org/mct/article-pdf/doi/10.1158/1535-7163.MCT-21-1021/3208456/mct-21-1021.pdf by Instytut Marii Sklodowskiej-Curie Oddzial w. Gliwicach user on 10 October 2022

38. Akizawa H, Imajima M, Hanaoka H, Uehara T, Satake S, Arano Y. Renal brush border enzyme-cleavable linkages for low renal radioactivity levels of radiolabeled antibody fragments. Bioconjug Chem. 2013;24:291–9.

39. Vaidyanathan G, Kang CM, McDougald D, Minn I, Brummet M, Pomper MG, et al. Brush border enzyme-cleavable linkers: evaluation for reducing renal uptake of radiolabeled prostate-specific membrane antigen inhibitors. Nucl Med Biol. 2018;62-63:18–30.

40. Zhou Z, Devoogdt N, Zalutsky MR, Vaidyanathan G. An efficient method for labeling single domain antibody fragments with ^{18}F using tetrazine-trans-cyclooctene ligation and a renal brush border enzyme-cleavable linker. Bioconjug Chem. 2018;29:4090–103.

41. Gainkam LO, Caveliers V, Devoogdt N, Vanhoce C, Xavier Cet al. Localization, mechanism and reduction of renal retention of technetium-99m labeled epidermal growth factor receptor-specific nanobody in mice. Contrast Media Mol Imaging. 2011;6:85–92.

42. Geenen L, Nonnekens J, Konijnenberg M, Baatout S, De Jong M, Aerts A. Overcoming nephrotoxicity in peptide receptor radionuclide therapy using [^{177}Lu]Lu-DOTA-TATE for the treatment of neuroendocrine tumours. Nucl Med Biol. 2021;102–103:1–11.

Downloaded from http://aacrjournals.org/mct/article-pdf/doi/10.1158/1535-7163.MCT-21-1021/3208456/mct-21-1021.pdf by Instytut Marii Sklodowskiej-Curie Oddzial w. Gliwicach user on 10 October 2022

Table 1. *Ex vivo* time-dependent biodistribution of [^{225}Ac]Ac-DOTA-2Rs15d co-infused with 150 mg/kg Gelofusine in a s.c. HER2^{pos} mouse tumor model (n = 3). Results are presented as mean % IA/g ± SD. Dosimetry data are expressed as mGy/kBq.

	Ex Vivo Biodistribution									Dosimetry	
Tissue / organ	**1h**	**3h**	**6h**	**24h**	**48h**	**72h**	**96h**	**120h**	**168h**	**Absorbed Dose [mGy/kBq]**	**Absorbed Dose × RBE factor (5) [mGy/kBq]**
Liver	0.66±0.02	0.81±0.19	0.32±0.09	0.79±0.08	0.63±0.01	0.52±0.13	0.40±0.11	0.44±0.04	0.41±0.18	13.56	67.80
Spleen	0.25±0.14	0.33±0.02	0.17±0.14	0.41±0.07	0.23±0.07	0.15±0.06	0.16±0.02	0.12±0.01	0.15±0.01	5.10	25.50
Lungs	0.15±0.05	0.09±0.01	0.05±0.03	0.06±0.02	0.07±0.01	0.03±0.03	0.02±0.01	0.03±0.01	0.04±0.01	1.08	5.40
Heart	0.10±0.02	0.06±0.02	0.05±0.01	0.10±0.04	0.06±0.04	0.05±0.04	0.05±0.05	0.06±0.05	0.06±0.03	1.59	7.95
Stomach	0.14±0.03	0.11±1.07	0.04±0.00	0.05±0.03	0.04±0.02	0.03±0.00	0.03±0.01	0.02±0.01	0.04±0.01	0.97	4.85
Kidneys	8.98±3.30	11.69±1.1	10.31±0.6	6.08±0.27	4.13±0.20	2.80±0.71	1.93±0.13	3.35±1.03	1.91±1.15	103.50	517.50
Lg. Int.	0.05±0.03	0.08±0.01	0.04±0.00	0.05±0.01	0.04±0.01	0.01±0.01	0.01±0.01	0.02±0.01	0.02±0.00	0.62	3.10
Sm. Int.	0.07±0.01	0.05±0.00	0.04±0.01	0.03±0.00	0.01±0.02	0.02±0.01	0.01±0.02	0.01±0.00	0.01±0.01	0.44	2.20
Pancreas	0.04±0.02	0.03±0.00	0.08±0.11	0.03±0.02	0.02±0.00	0.02±0.00	0.01±0.01	0.01±0.00	0.02±0.00	0.57	2.85
Muscle	0.08±0.03	0.03±0.01	0.04±0.01	0.02±0.02	0.01±0.01	0.02±0.01	0.02±0.00	0.03±0.01	0.04±0.02	0.64	3.20
Blood	0.23±0.20	0.01±0.01	0.01±0.00	0.14±0.21	0.13±0.23	0.05±0.08	0.23±0.36	0.07±0.04	0.18±0.00	2.55	12.75
Bone	0.29±0.06	0.10±0.01	0.09±0.04	0.36±0.06	0.32±0.10	0.06±0.02	0.06±0.01	0.05±0.06	0.08±0.03	3.62	18.10
Tumor	8.36±0.23	9.64±1.69	9.87±1.38	6.58±1.78	6.20±1.00	4.24±0.68	3.73±0.58	1.70±0.64	2.24±1.00	115.58	577.90
T-to-Liver	12.62±0.73	12.08±1.71	33.40±12.13	8.29±1.59	9.79±1.61	8.31±1.10	9.60±1.23	3.78±1.06	5.60±0.66	-	-
T-to-Kidneys	1.03±0.42	0.82±0.13	0.95±0.08	1.08±0.30	1.50±0.22	1.55±0.24	1.92±0.18	0.60±0.46	1.54±1.32	-	-

Downloaded from http://aacrjournals.org/mct/article-pdf/doi/10.1158/1535-7163.MCT-21-1021/3208456/mct-21-1021.pdf by Instytut Marii Sklodowskiej-Curie Oddzial w. Gliwicach user on 10 October 2022

Table 2. Histopathological analysis of kidneys sections from mice enrolled in the dose-escalation study. Kidney sections were stained with H&E. Incidence and Mean Severity of Findings in Kidney. GRADE 1 = Minimal, GRADE 2 = Slight, GRADE 3 = Moderate, GRADE 4 = Marked, GRADE 5 = Severe; description of the severity scores is detailed in the Supplementary Material.

	Groups [kBq]			
	Control (0 kBq)	**19 kBq**	**38 kBq**	**75 kBq**
Total Animals	3	3	3	3
Tubular cast, hyaline	1/1.0	2/2.0	3/1.6	3/1.3
Tubular basophilia	1/1.0	0	0	0
Tubular dilation	0	3/2.6	3/3.3	3/2.6
Cytoplasmic vacuolation	0	3/2.6	3/3.0	3/2.6
Tubular necrosis	0	3/3.0	3/3.6	3/3.3
Tubular regeneration	0	3/4.0	3/5.0	3/4.3
Fibrosis interstitial	0	3/3.0	3/3.0	3/3.6
Inflammation	2/1.0	3/2.0	3/2.0	3/2.6
Mononuclear foci	1/1.0	2/2.0	3/1.6	3/1.0
Karyomegaly	0	3/1.3	3/1.3	3/2.0
Glomerular atrophy	0	3/1.3	2/1.5	3/2.0
Mineralization	0	1/2.0	0	1/1.0
Pelvis dilation	1/1.0	0	0	0

Figure 1. Cytotoxic activity of (i) [^{225}Ac]Ac-DOTA-2Rs15d alone or (ii) blocked with cold 2Rs15d; and (iii) non-targeting [^{225}Ac]Ac-DOTA-R3B23 control probe on SKOV-3 cells determined via clonogenic (**A-B**) and DNA double-strand-break (**C-D**) assays. Representative images (**A**) and survival fractions (SF) (**B**) of SKOV-3 cells from clonogenic assay. **C,** The average number of γH2AX-foci quantified per cell; NT - control cells non-treated with radioactivity. **D,** Representative images of detected γH2AX-foci in treated SKOV-3 cells.

Downloaded from http://aacrjournals.org/mct/article-pdf/doi/10.1158/1535-7163.MCT-21-1021/3208456/mct-21-1021.pdf by Instytut Marii Sklodowskiej-Curie Oddzial w. Gliwicach user on 10 October 2022

Figure 2. *In vivo* specificity of [^{225}Ac]Ac-DOTA-2Rs15d alone or blocked with excess of cold 2Rs15d, and non-targeting [^{225}Ac]Ac-DOTA-R3B23 after 1 h p.i. in s.c. SKOV-3 tumor-xenografted mice (**A**). *, P< 0.00015; **, P< 0.00004; ***, P< 0.000003. **B,** Time-dependent biodistribution of [^{225}Ac]Ac-DOTA-2Rs15d in a s.c. SKOV-3 tumor-xenografted mouse model. **C-F,** Dose-escalation study of [^{225}Ac]Ac-DOTA-2Rs15d in healthy C57Bl/6 mice with Kaplan-Meier survival plots (**C**) and relative body weight (**D**) in various groups of treated mice. Histopathological analysis of kidney's sections from mice receiving only vehicle solution 0.9% NaCl (**E**) and 19 kBq of [^{225}Ac]Ac-DOTA-2Rs15d (**F**).

Figure 3. α-camera imaging of [^{225}Ac]Ac-DOTA-2Rs15d activity distribution in cryo-sectioned HER2^{pos} tumors (**A**) and kidneys (**B**) of s.c. SKOV-3 xenografts. All images were taken at 1, 4 and 24 h p.i. **C,** Histogram of the activity distribution of an α-camera image of kidneys 4 h p.i. derived from ROIs encompassing the whole kidney area, including both cortex and medulla. **D,** Multi-term gaussian plots fitted to the histogram data of cortex ROI. Homogeneity of cortex (**E**) and tumor (**F**) was assessed by plots where the total signal fraction is displayed as a function of the total area fraction. A completely uniform ROI corresponds to a linear function (depicted as a dashed line) and an area under the curve (AUC) of 0.5.

Figure 4. Therapy with [^{225}Ac]Ac-DOTA-2Rs15d improves survival of mice bearing disseminated intraperitoneal SKOV3.IP1 tumors. Treatment schedules (**A**) and Kaplan-Meier survival plots (**B**) together with relative body weight (**C**) in various groups of treated mice. **D,** Calculated absorbed doses (Gy), without considering of RBE factor 5 for α-particles, in normal organs and tumor for one single therapeutic injection 85 kBq and total therapeutic activity 255 kBq of [^{225}Ac]Ac-DOTA-2Rs15d. H&E sections of kidneys from mice receiving 0.9% NaCl (**E**), one single dose (**F**) and three injections (**G**) of [^{225}Ac]Ac-DOTA-2Rs15d.

Downloaded from http://aacrjournals.org/mct/article-pdf/doi/10.1158/1535-7163.MCT-21-1021/3208456/mct-21-1021.pdf by Instytut Marii Sklodowskiej-Curie Oddzial w. Gliwicach user on 10 October 2022

FIGURE 1

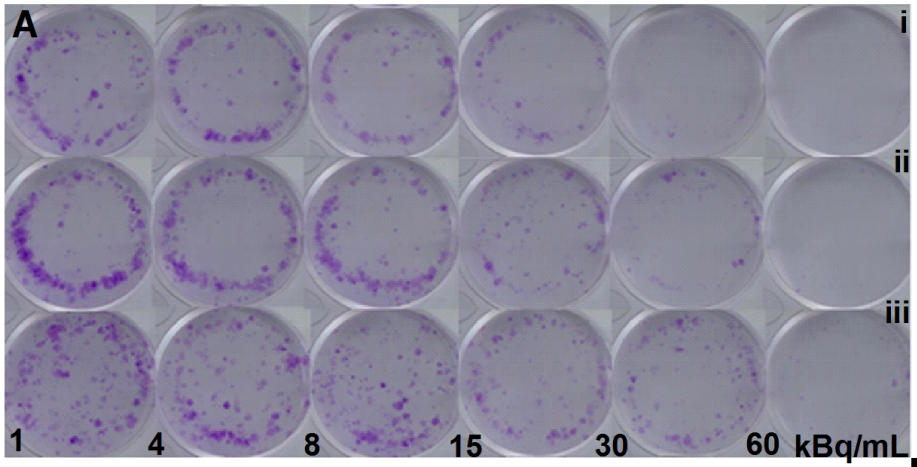

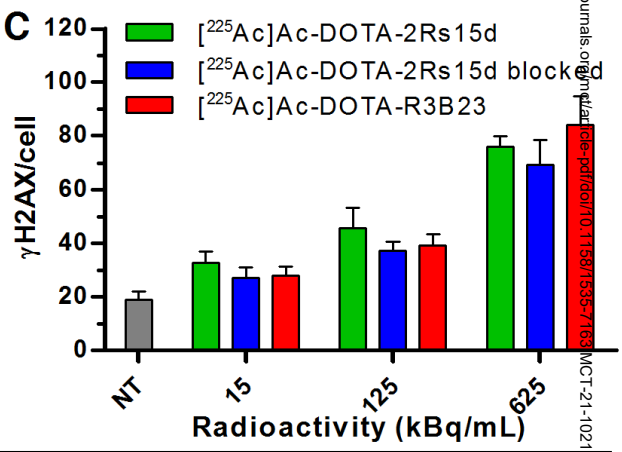

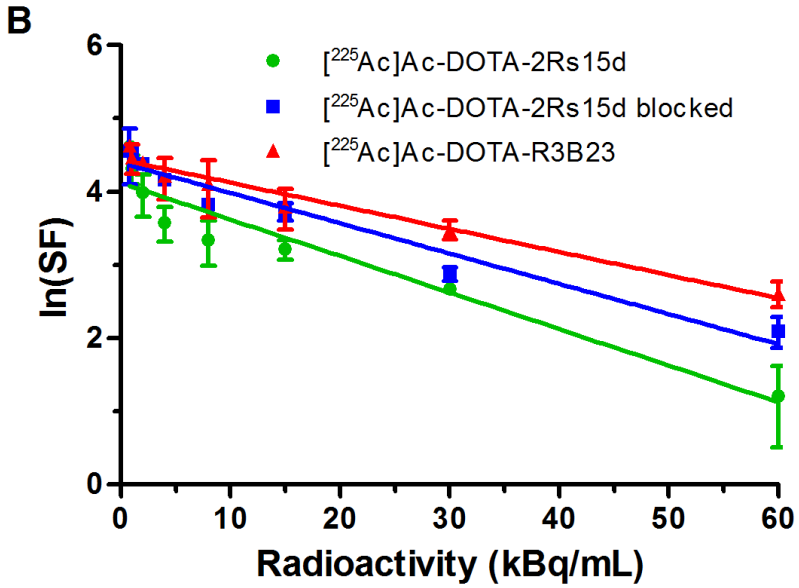

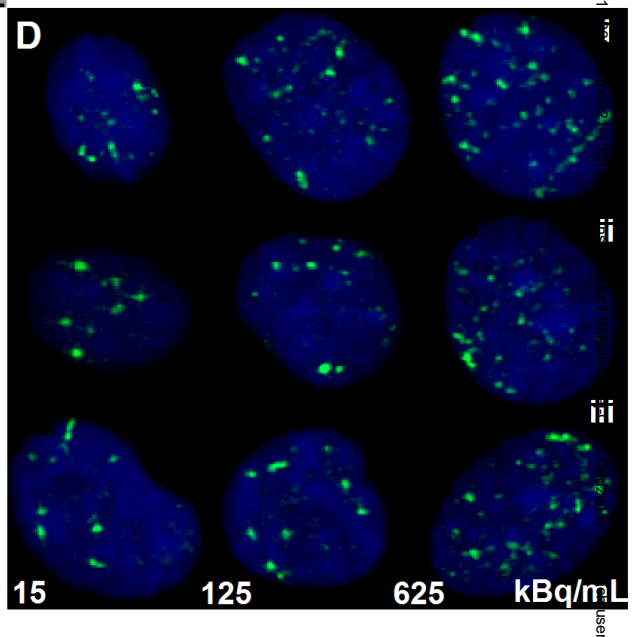

Downloaded from http://aacrjournals.org/mct/article-pdf/doi/10.1158/1535-7163.MCT-21-1021 by guest user on 10 October 2022

FIGURE 2

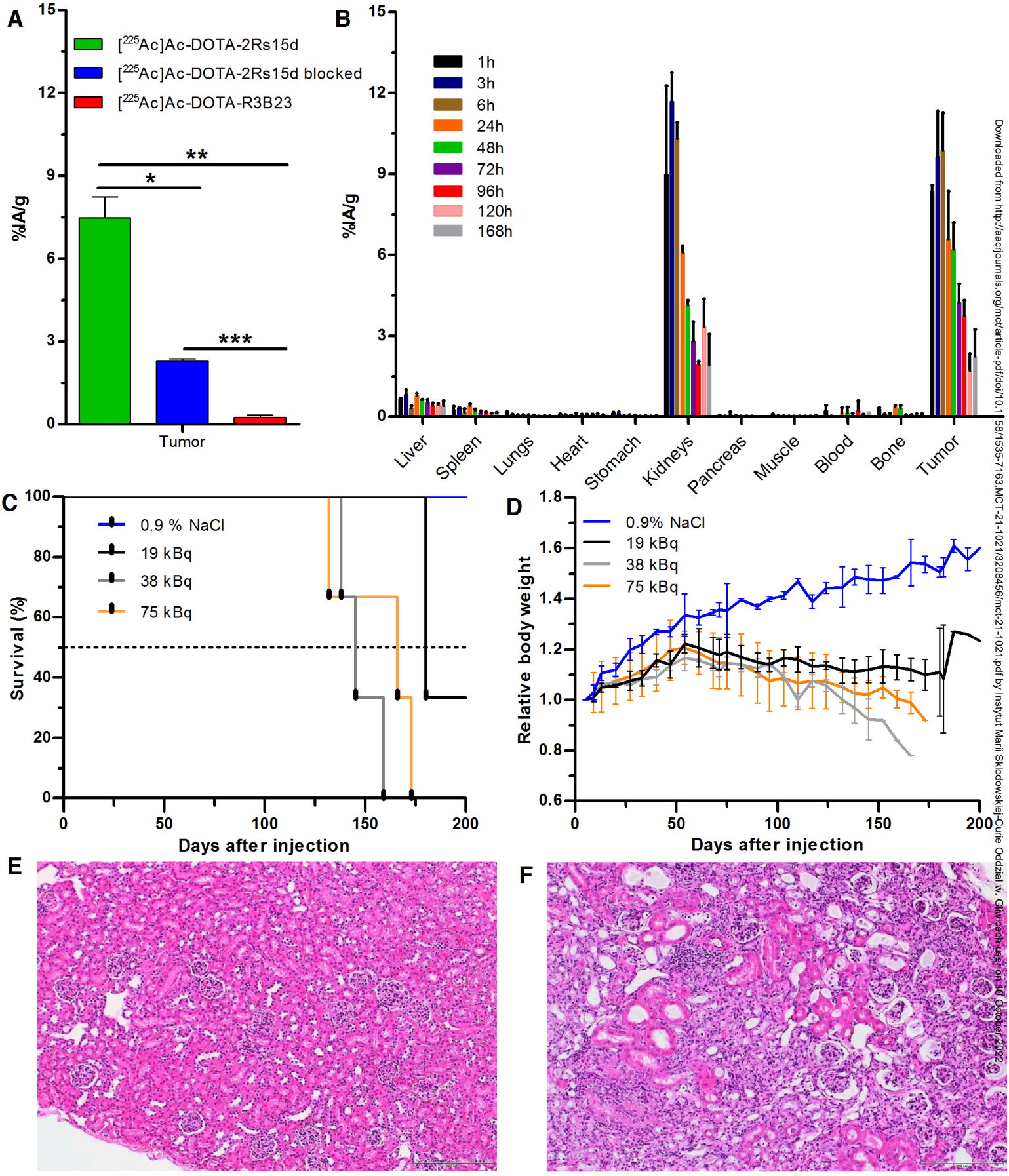

Downloaded from http://aacrjournals.org/mct/article-pdf/doi/10.1158/1535-7163.MCT-21-1021/3208456/mct-21-1021.pdf by Instytut Marii Sklodowskiej-Curie Oddzial w. Gliwicach user on 10 October 2022

FIGURE 3

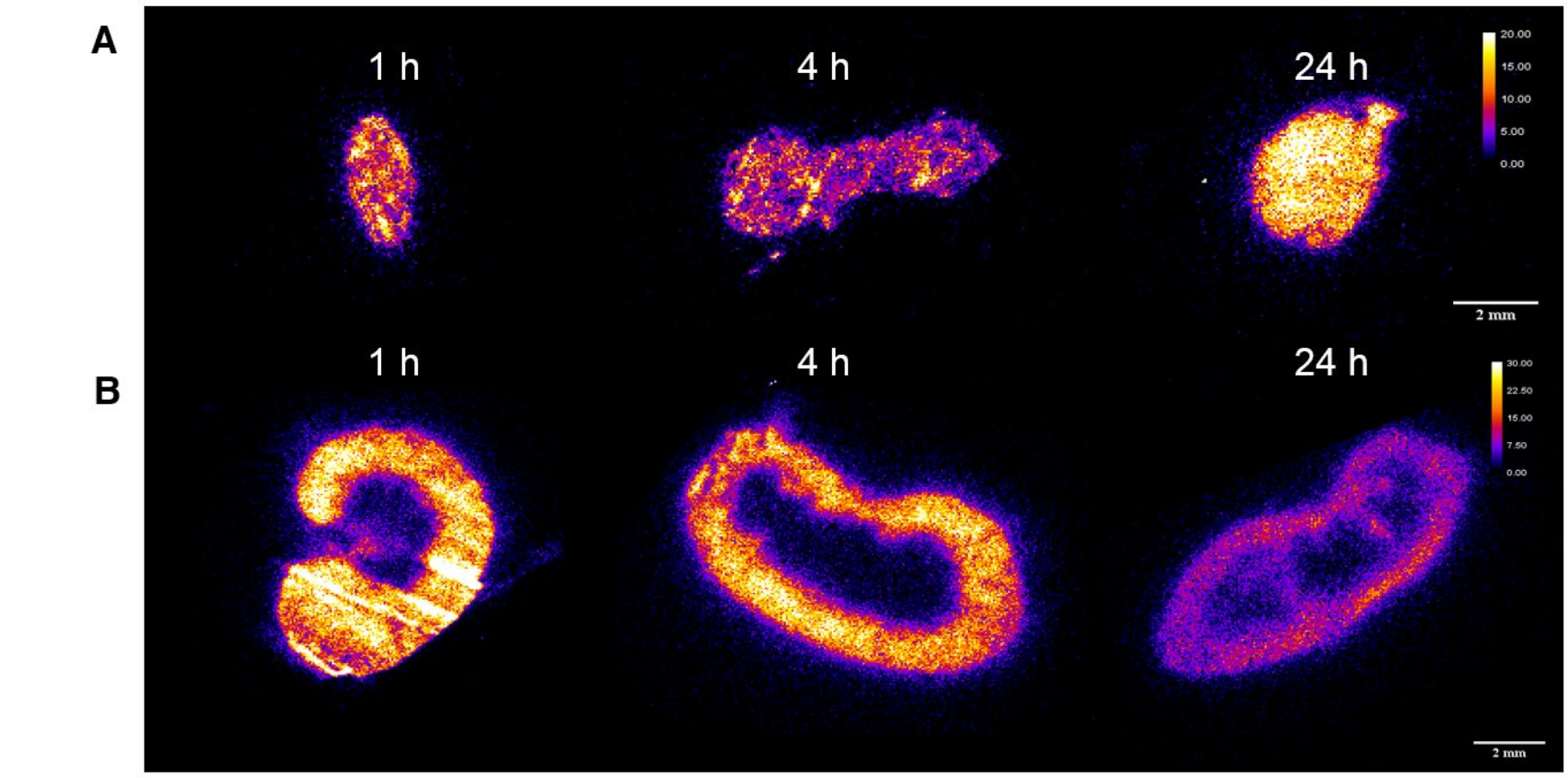

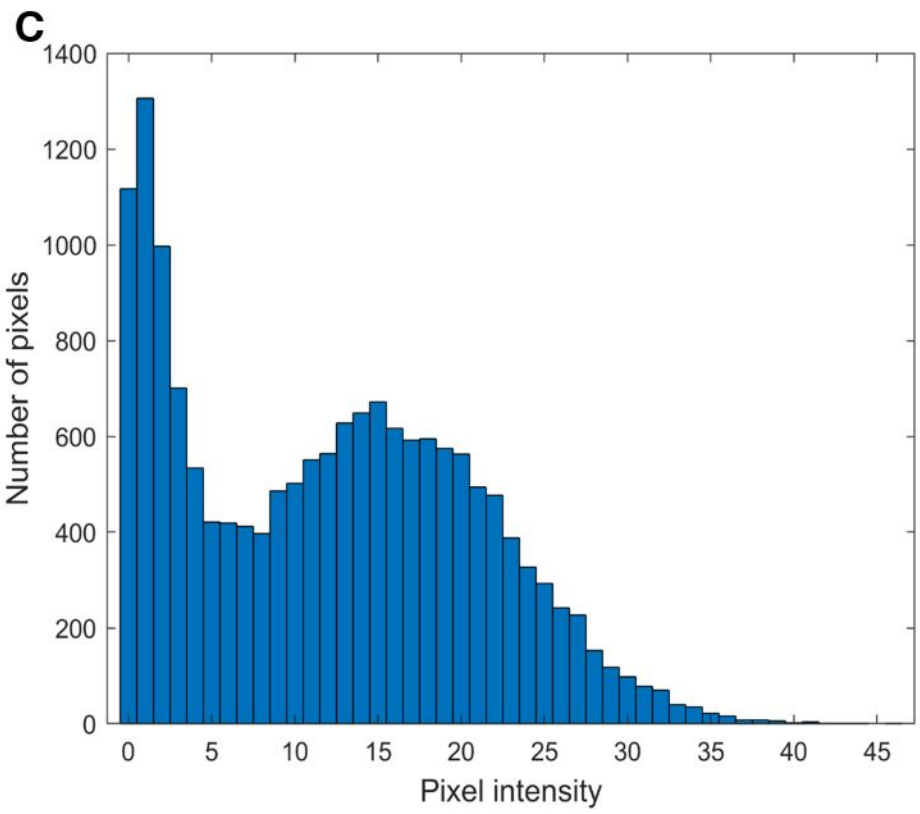

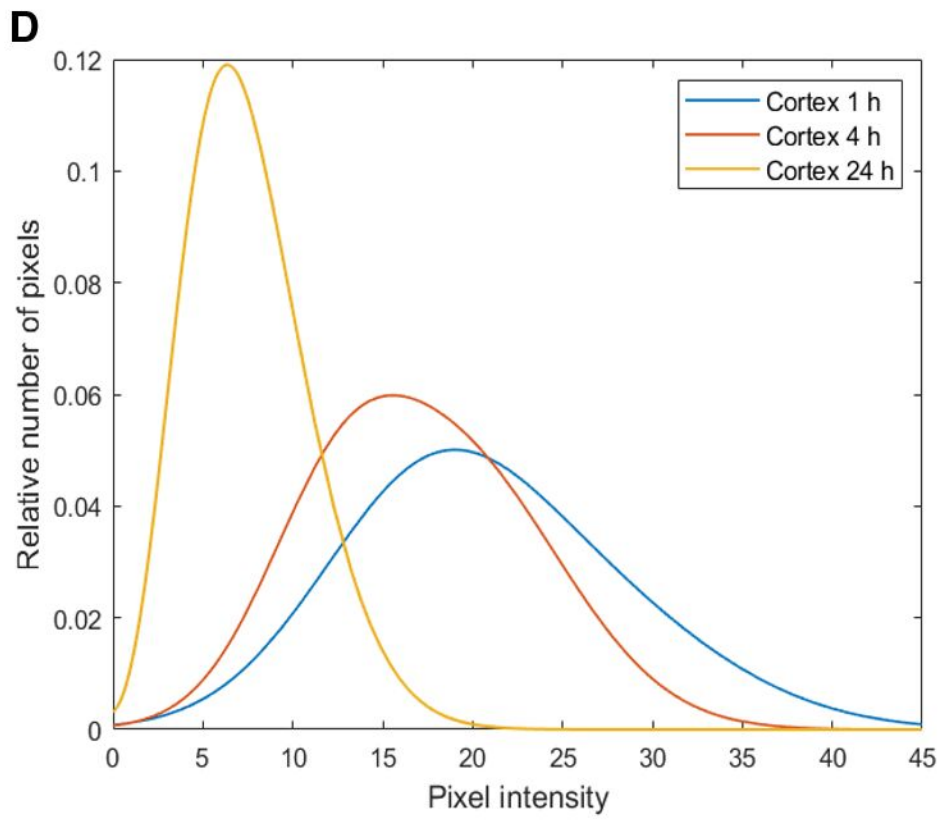

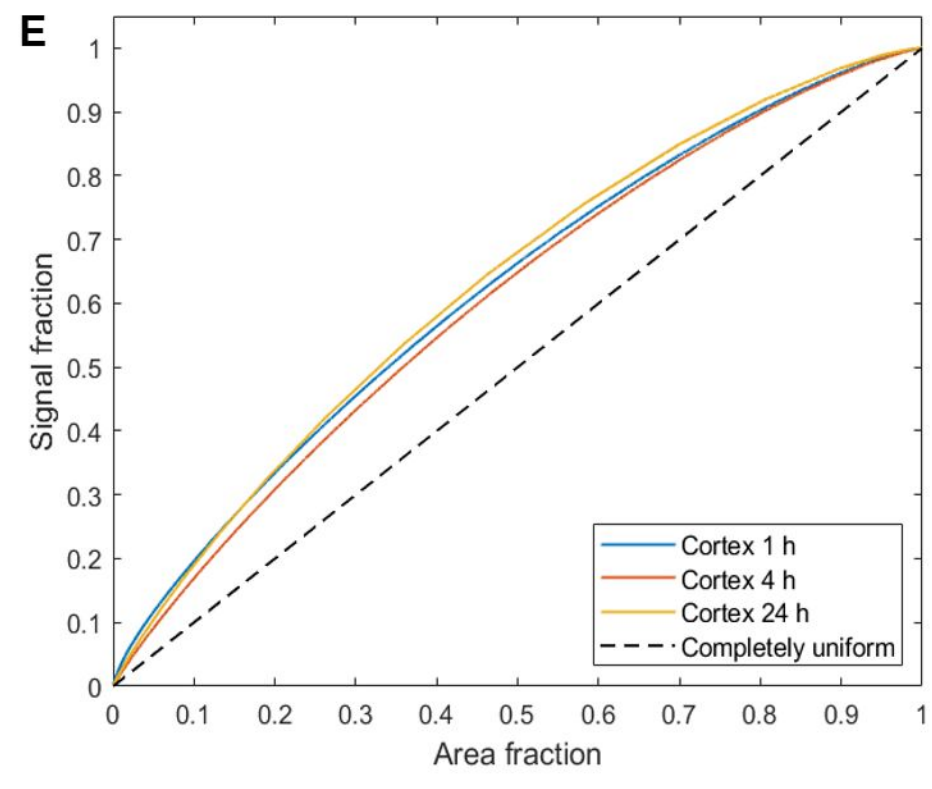

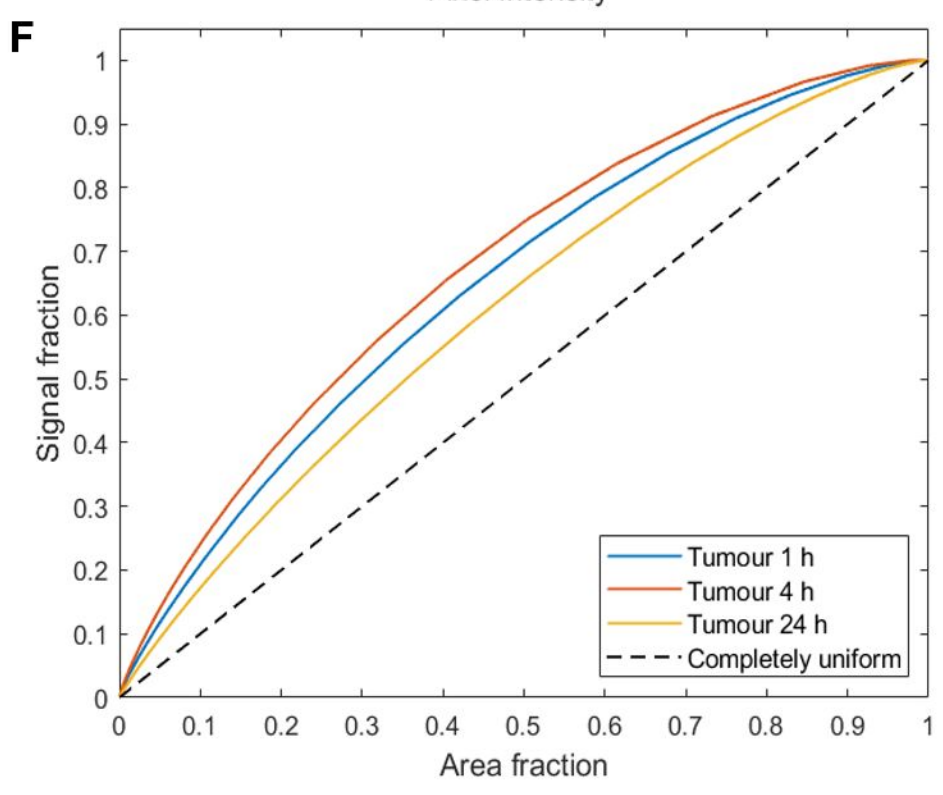

Downloaded from http://aacrjournals.org/mct/article-pdf/doi/10.1158/1535-7163.MCT-21-1021/3208456/mct-21-1021.pdf by Instytut Marii Sklodowskiej-Curie Oddzial w. Gliwicach user on 10 October 2022

FIGURE 4

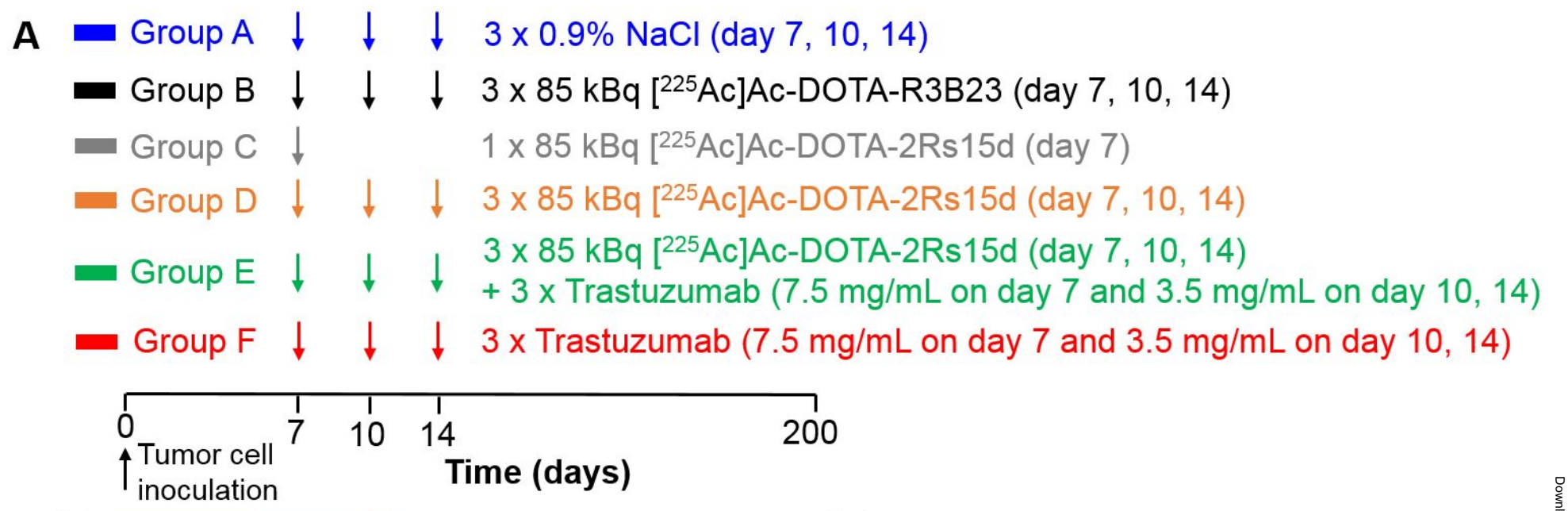

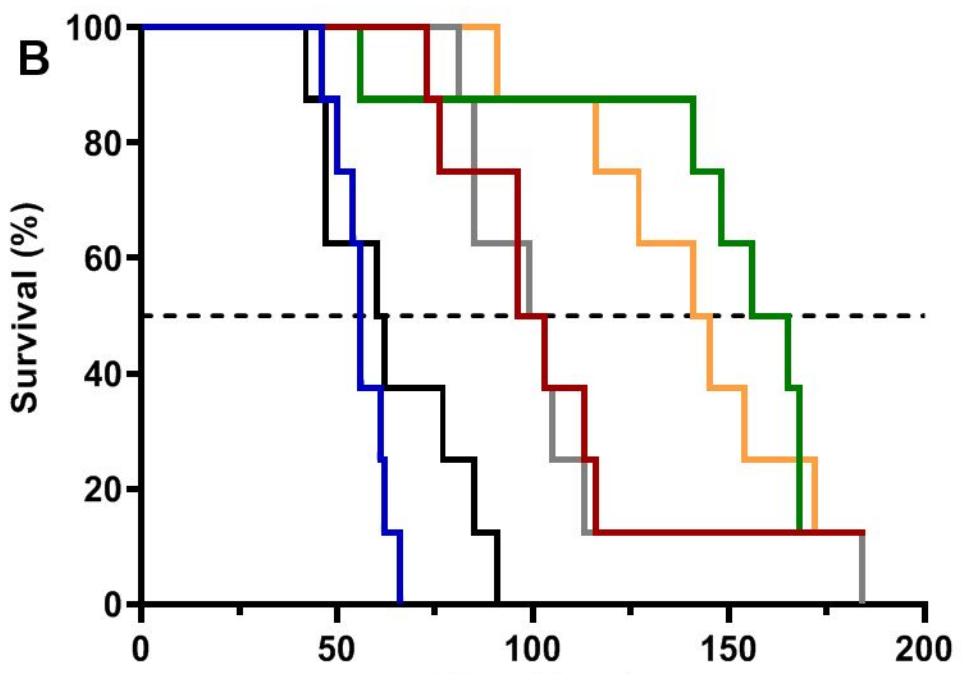

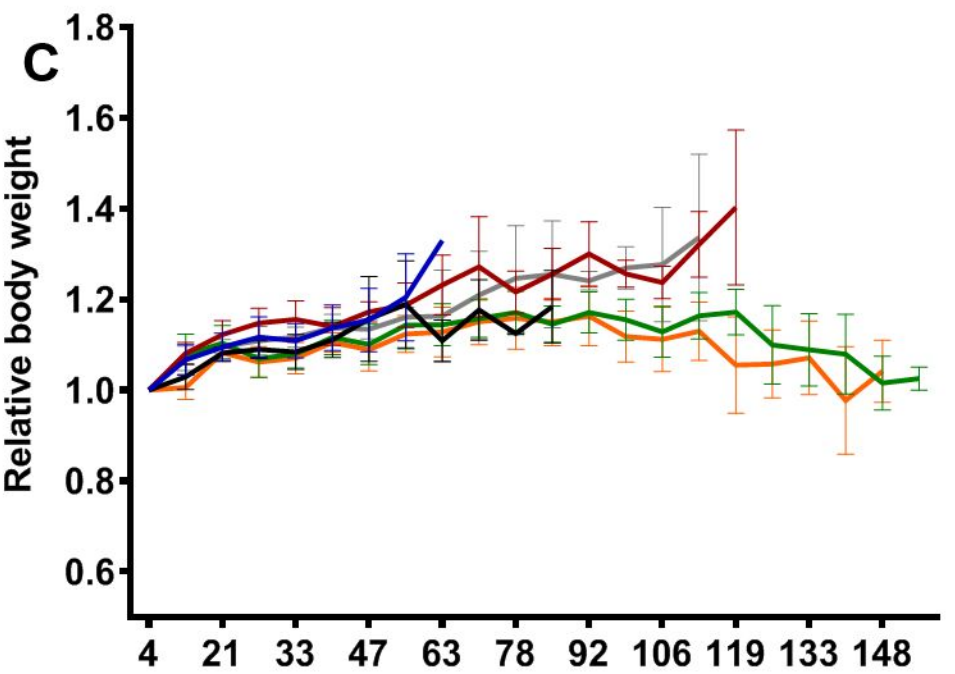

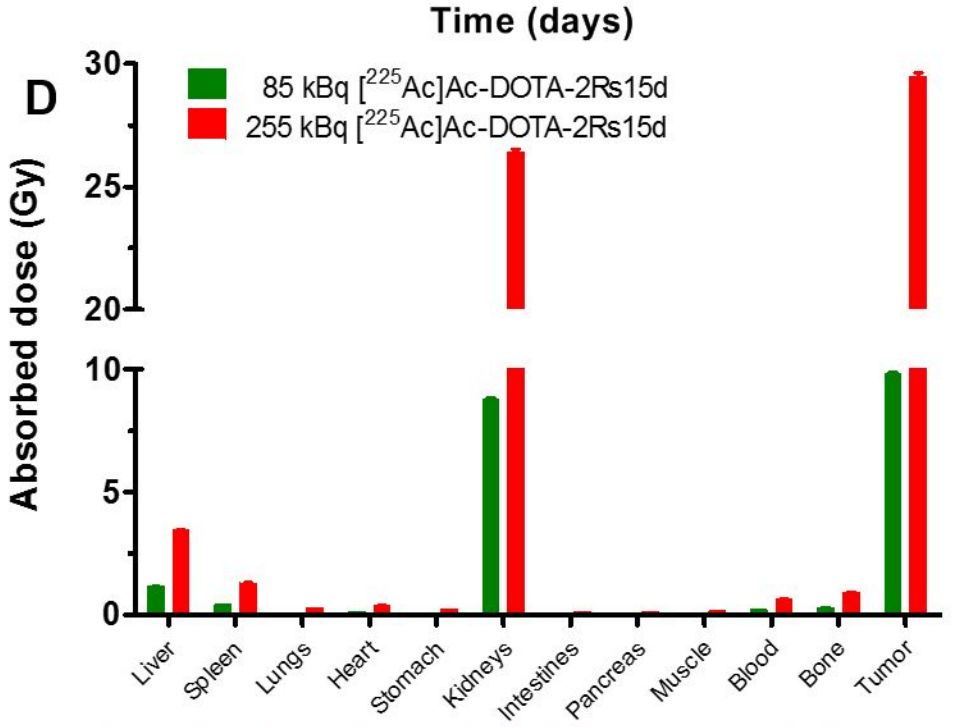

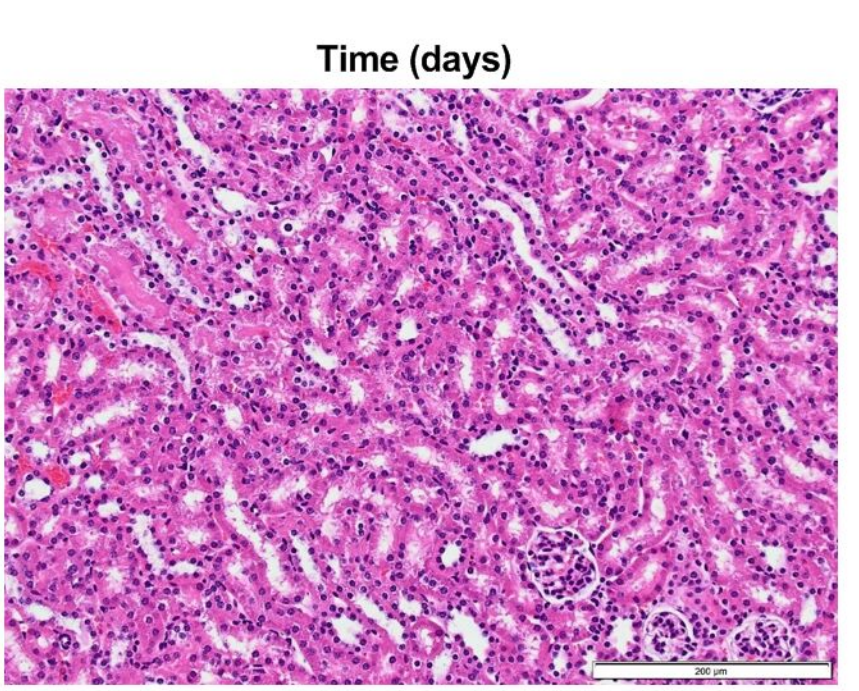

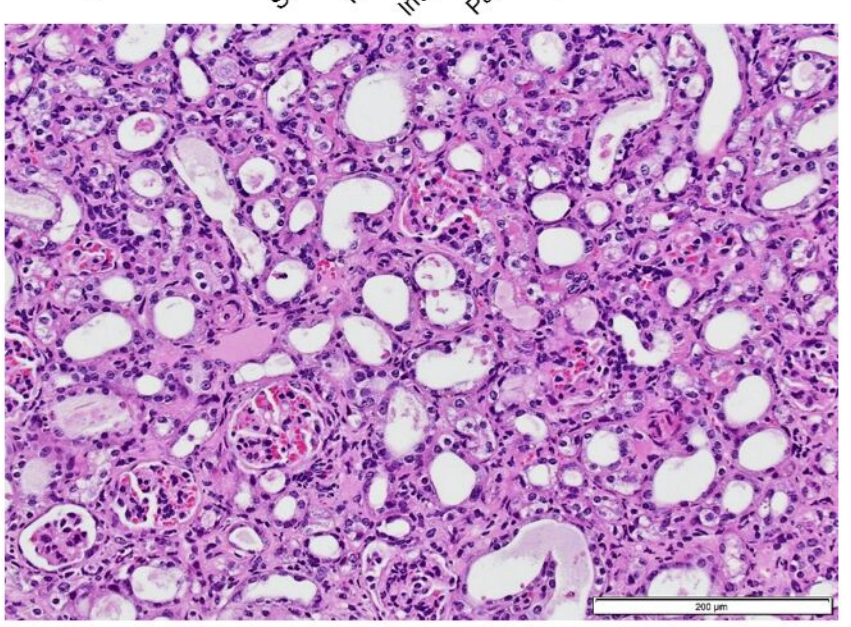

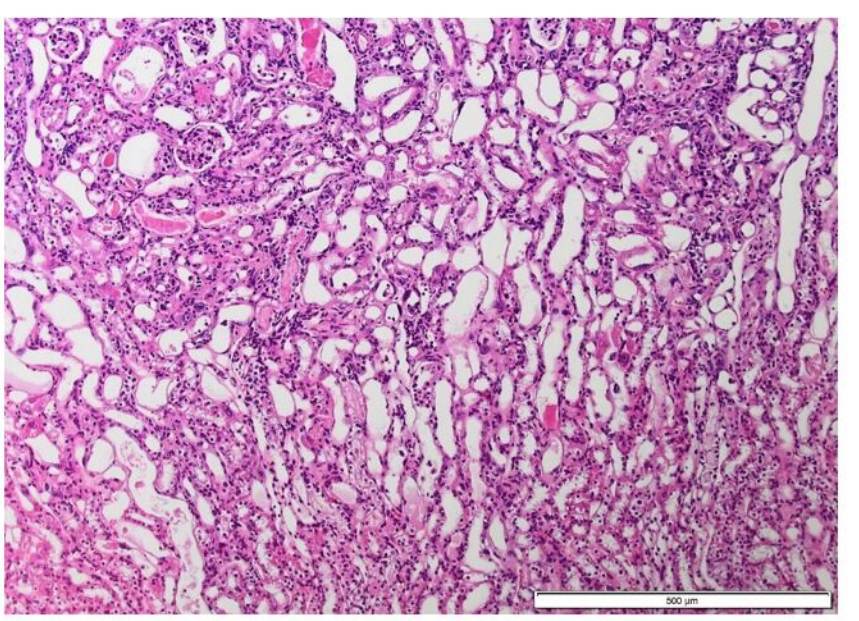

Downloaded from http://aacrjournals.org/mct/article-pdf/doi/10.1158/1535-7163.MCT-21-1021/3208456/mct-21-1021.pdf by Instytut Marii Sklodowskiej-Curie Oddzial w. Gliwicach user on 10 October 2022